Ionic Liquid Pre-intercalated MXene Films for Ionogel-based Flexible Micro-Supercapacitors with High Volumetric Energy Density

Shuanghao Zheng,‡[abc] Chuanfang (John) Zhang,‡[d] Feng Zhou,[a] Yanfeng Dong,[a] Xiaoyu Shi,[abe] Valeria Nicolosi,[d] Zhong-Shuai Wu*[a] and Xinhe Bao[ab]

[a] Dalian National Laboratory for Clean Energy, Dalian Institute of Chemical Physics, Chinese Academy of Sciences, 457 Zhongshan Road, Dalian 116023, China

*E-mail: wuzs@dicp.ac.cn (Z.-S.Wu)

[b] State Key Laboratory of Catalysis, Dalian Institute of Chemical Physics, Chinese Academy of Sciences, 457 Zhongshan Road, Dalian 116023, China

[c] University of Chinese Academy of Sciences, 19 A Yuquan Rd, Shijingshan District, Beijing, 100049, China

[d] CRANN & AMBER, School of Chemistry, Trinity College Dublin, Dublin 2, Ireland

[e] Department of Chemical Physics, University of Science and Technology of China, 96 JinZhai Road, Hefei 230026, China

‡ These authors contributed equally to this work.

Experimental Section

Synthesis of $Ti_3C_2T_X$ MXene: $Ti_3C_2T_X$ MXene was synthesized from the Ti_3AlC_2 by LiF/HCl etchants previously reported.[1-3]Typically, LiF (0.5 g) was dissolved into 9 M HCl (10 mL) under stirring. Then, Ti_3AlC_2 (0.5 g) was slowly added into the above solution with continuous stirring to avoid overheat. The resultant mixture was stirred at 35 ^oC for 24 h. Subsequently, the etched product was washed with deionized water through centrifugation (3500 rpm, 5 min) several times until pH reached up to 6 and the multilayer $Ti_3C_2T_X$ sediment was obtained. Afterwards, the obtained sediment was mixed with deionized water (10 mL) and the resulting mixture was subjected to vigorous shaking via vortex machine. Successively, the obtained dispersion was centrifuged (1500 rpm, 1 h) and then the collected sediment was subjected to higher centrifugation (3500 rpm, 1 h). After the resultant sediment was redispersed in deionized water under a vigorous shaking, $Ti_3C_2T_X$ MXene aqueous dispersion with a concentration of 0.65 mg mL^{-1} was achieved for further usage.

Fabrication of PM-MSCs: PM-MSCs were fabricated via layer-by-layer deposition of EG and MXene dispersion with assistance of a customized interdigital mask, followed by transfer process. Typically, alcohol dispersion of EG (2 mL, 0.1 mg mL^{-1}), prepared by electrochemical exfoliation of graphite at aqueous solution,[4,5] was uniformly filtrated through a customized interdigital mask (length of 14 mm, width of 1 mm, interspace of 500 μm) to form a thin interdigital EG layer on a PVDF membrane (pore size of 0.2 μm), helpful for the latter formation of MXene film and transfer process. Then, MXene aqueous solution (1.6 mL, 0.65 mg mL^{-1}) was

deposited on the interdigital EG layer. Note that the thickness of the MXene microelectrodes can be readily controlled by changing the volume of MXene solution. After the removal of mask, the as-fabricated interdigital microelectrodes were fully transferred onto PET substrate with the assistance of 20 MPa. To achieve ionic liquid pre-intercalated MXene film, the as-obtained undried MXene microelectrodes were directly immersed into the tested ionic liquid electrolyte for 24 h under vacuum. Finally, the corresponding electrolyte, e.g., $EMIMBF_4$, $EMIMBF_4$/PVDF-HFP, was drop-casted onto the project area of interdigital microelectrodes, and high-voltage ionic liquid or ionogel based PM-MSCs were achieved after Kapton tape package. For comparison, DM-MSCs were also fabricated based on completely dried MXene film, obtained by drying treatment of freshly undried MSCs at 120 ^{o}C for 24 h under vacuum, while other steps kept the same as the PM-MSCs.

$EMIMBF_4$/PVDF-HFP Ionogel Electrolyte: Ionogel electrolyte was prepared as the following steps.[19] First, PVDF-HFP (0.2 g) was dissolved at acetone (2 mL) under stirring to form transparent solution. Then, $EMIMBF_4$ (1.8 g) was dropwise added into the above solution. After stirring 2 h, $EMIMBF_4$/PVDF-HFP ionogel electrolyte was obtained. Finally, the ionogel electrolyte was carefully drop-casted on the project area of microelectrodes and solidified in vacuum drying oven at 80 ^{o}C for 24 h.

Material Characterization: The morphology and structure of MXene and micro-electrodes were carried out at SEM (JSM-7800F), high-resolution transmission electron microscopy (HRTEM, JEM-2100), XRD (X`pert Pro), atomic force microscopy (AFM, Asylum Research MFP). The electrical conductivity of

micro-electrodes was measured at four-point probe equipment (RTS-9). The thickness and surface profile mapping were performed at stylus profiler (Alpha step D-600).

Electrochemical Measurements: The electrochemical performances were recorded at the electrochemical workstation (CHI760E). CV curves were tested from 10 to 500 mV s^{-1}. GCD profiles were measured ranging from 0.1 to 2 mA cm^{-2}. EIS spectra were recorded with the frequency from 0.01 Hz to 100 kHz under a ac amplitude of 5 mV. LSV measurements was carried out at the architecture of stainless steel/electrolyte/stainless steel.

Calculation: Based on CV curves, the volumetric specific capacitance of the electrode was calculated from the following equation (1):

$$C_{Volume} = \frac{4}{vV(V_f - V_i)} \int_{V_i}^{V_f} I(V)dV \quad (1)$$

Where C_{volume} is the volumetric specific capacitance of single electrode (F cm^{-3}), v is scan rate (V s^{-1}), V is the total volume of two electrodes (cm^{-3}), V_f and V_i are the high and low potential of the CV curves, respectively, and $I(V)$ is the discharge current (A).

Based on GCD profiles, the capacitance of the fabricated MSCs was evaluated via the below formula (2):

$$C = \frac{It}{\Delta V} \quad (2)$$

Where C is the calculated value, I is discharged current from GCD profiles (A), t is discharged time (s). ΔV is discharged voltage window (V).

The areal capacitance and volumetric capacitance of single electrode were evaluated based on the areal and volume of single electrode according to the following formula (3) and (4):

$$C_{electrode}^{areal} = 4 \times C/A_{device} \quad (3)$$

$$C_{electrode}^{volume} = 4 \times C / V_{device} \quad (4)$$

Where $C_{electrode}^{areal}$ and $C_{electrode}^{volume}$ are the calculated areal capacitance and volumetric capacitance of single electrode, respectively. A_{device} (cm^{-2}) and V_{device} (cm^{-3}) are the total area and volume of two electrodes, respectively.

The areal and volumetric capacitance of device were calculated from the following equations (5) and (6):

$$C_{device}^{areal} = C/A_{device} \quad (5)$$

$$C_{device}^{volume} = C / V_{device} \quad (6)$$

Where C_{device}^{areal} and C_{device}^{volume} are the calculated areal capacitance and volumetric capacitance of the device, respectively.

The areal energy density and power density of the fabricated devices were evaluated based on the below equations (7) and (8):

$$E_{areal} = \frac{1}{2} \times C_{device}^{areal} \times \frac{(\Delta V)^2}{3600} \quad (7)$$

$$P_{areal} = \frac{E_{areal}}{t} \times 3600 \quad (8)$$

Where E_{areal} is the areal energy density, and P_{areal} is the areal power density.

The volumetric energy density and power density of the fabricated devices were calculated based on the below equations (9) and (10):

$$E_{volume} = \frac{1}{2} \times C_{device}^{volume} \times \frac{(\Delta V)^2}{3600} \quad (9)$$

$$P_{volume} = \frac{E_{volume}}{t} \times 3600 \quad (10)$$

Where E_{volume} is the volumetric energy density, and P_{volume} is the volumetric power density.

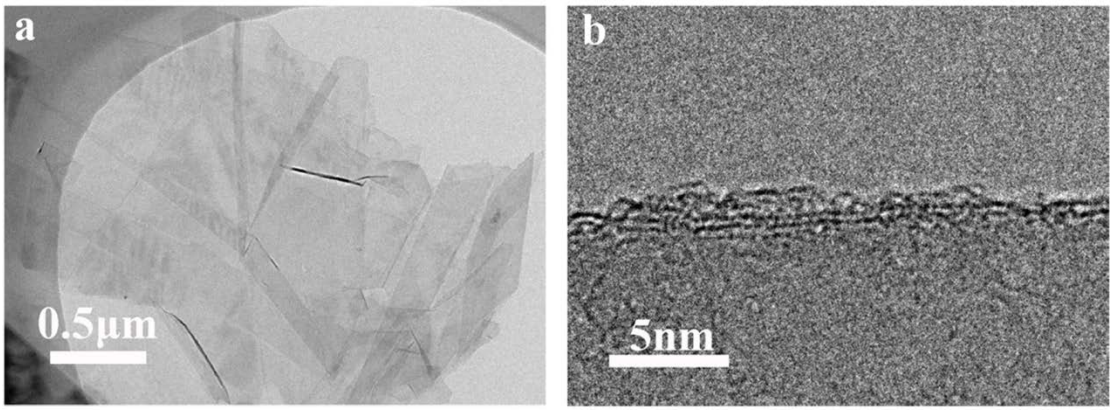

Fig. S1 (a) TEM image of EG nanosheets from cathodal exfoliation, showing microscale size of EG nanosheets. (b) HRTEM image, exhibiting double-layer EG nanosheets.

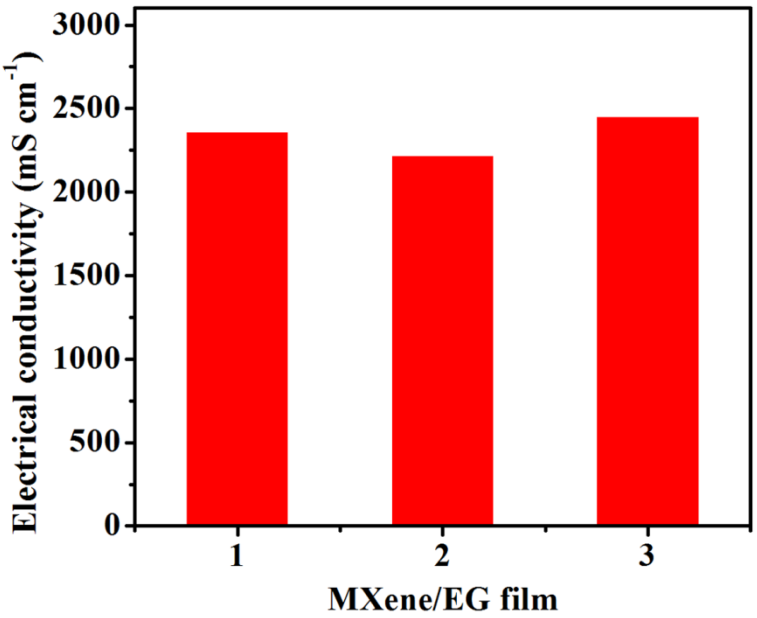

Fig. S2 The electrical conductivity of the fabricated microelectrode films tested at three different positions.

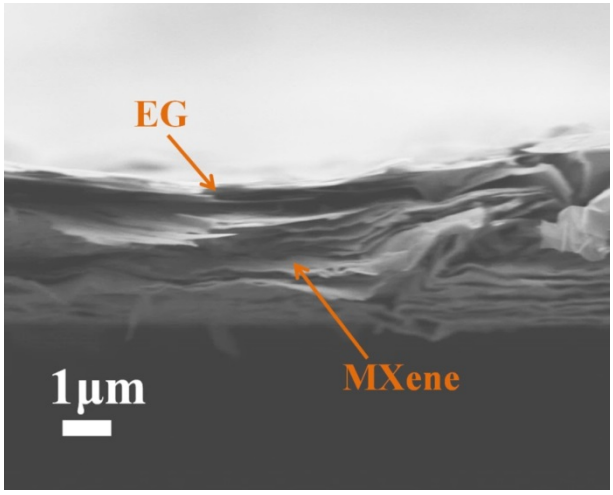

Fig. S3 Cross-section high-magnification SEM image of the microelectrode film.

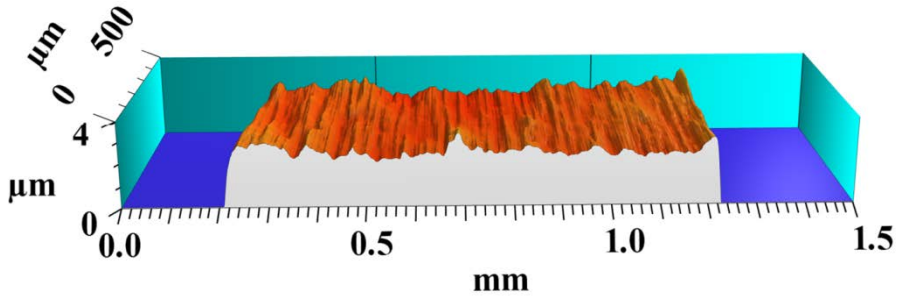

Fig. S4 3D view of the surface profile of the microelectrode finger on PET substrate, measured by Alpha step D-600.

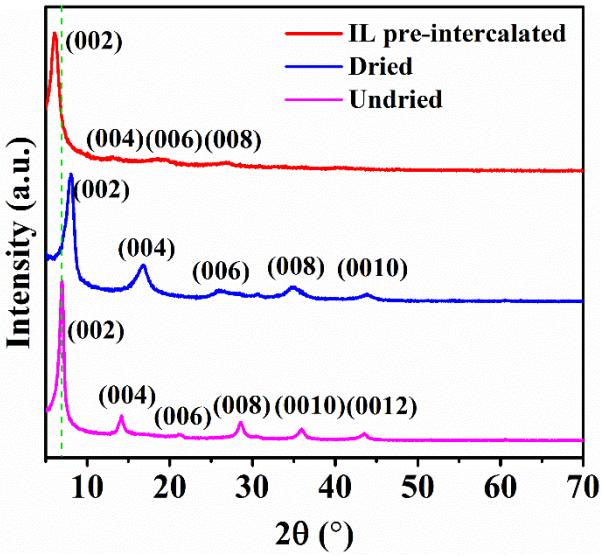

Fig. S5 XRD patterns of freshly undried, dried and $EMIMBF_4$ pre-intercalated films.

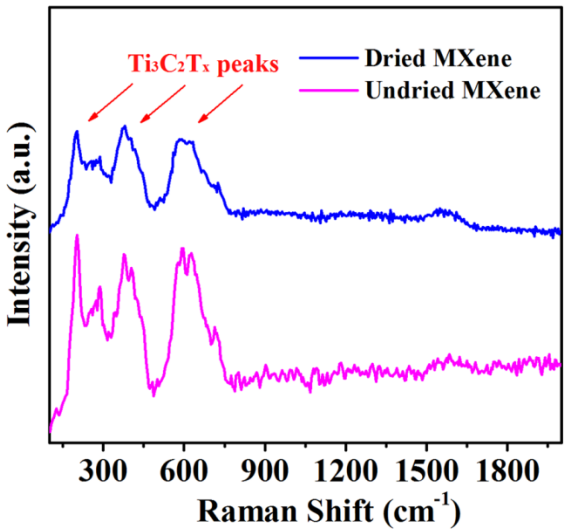

Fig. S6 Raman spectra of undried MXene and dried MXene at 120 °C under vacuum, showing no apparent change of characteristic peaks.

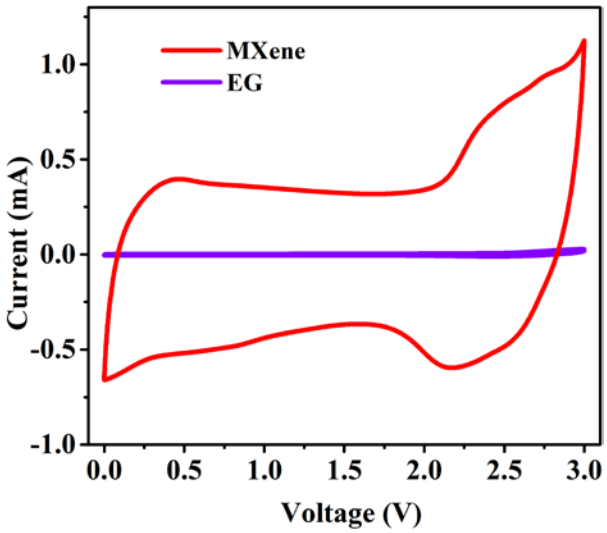

Fig. S7 CV curves of PM-MSCs, and MSCs based on pure EG film, tested at 50 mV s^{-1}.

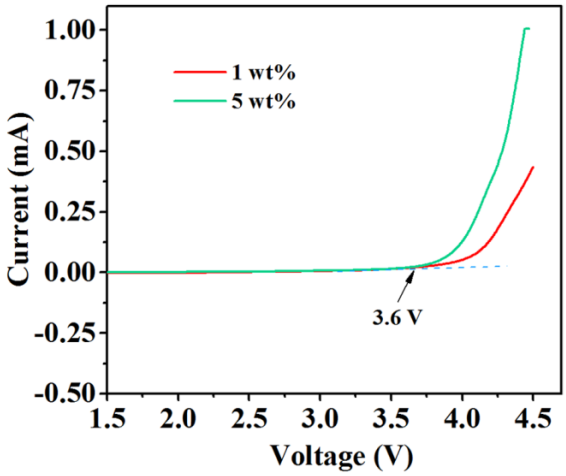

Fig. S8 LSV curves of $EMIMBF_4$ containing a water percent of 1 and 5 wt% at the scan rate of 5 mV s^{-1}.

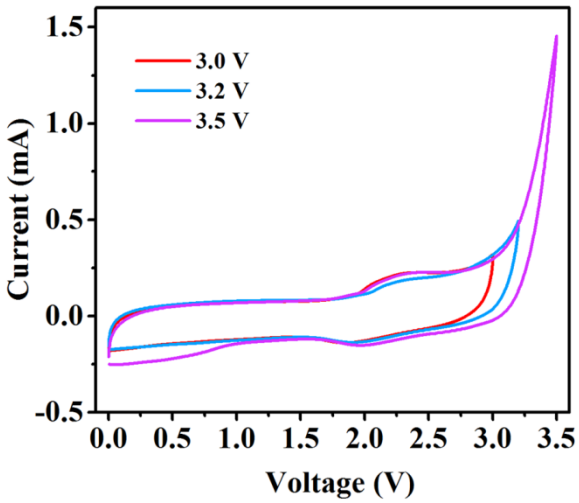

Fig. S9 CV curves of MXene based MSCs tested at various voltages of 3, 3.2 and 3.5 V at scan rate of 20 mV s^{-1}.

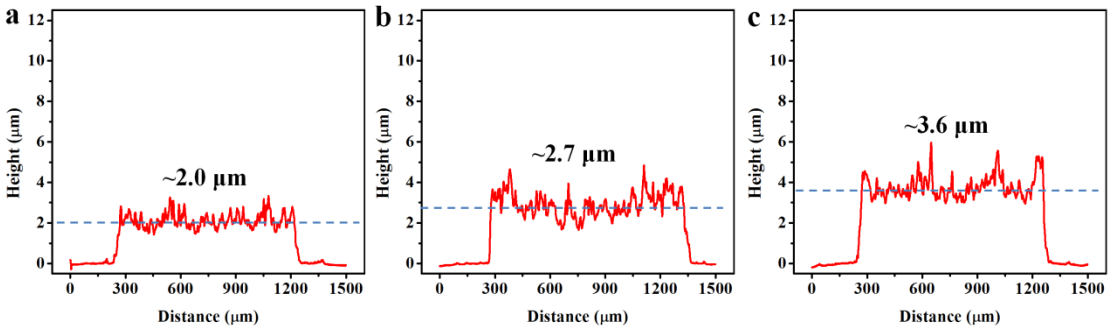

Fig. S10 Height profiles of microelectrode finger with the thickness of 2.0, 2.7 and 3.6 µm.

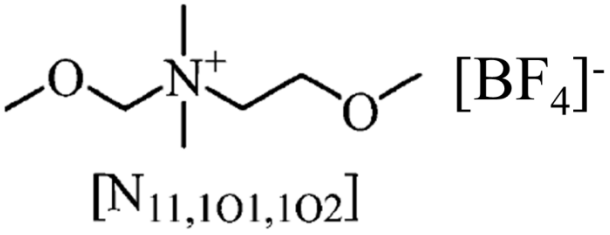

$[N_{11,1O1,1O2}]$

Fig. S11 Chemical structure of $N_{11,1O1,1O2}BF_4$.

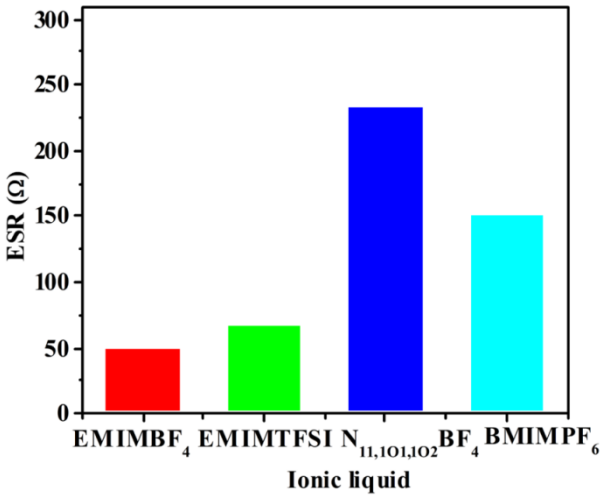

Fig. S12 ESR values of PM-MSCs-EB, PM-MSCs-ET, PM-MSCs-NB and PM-MSCs-BP.

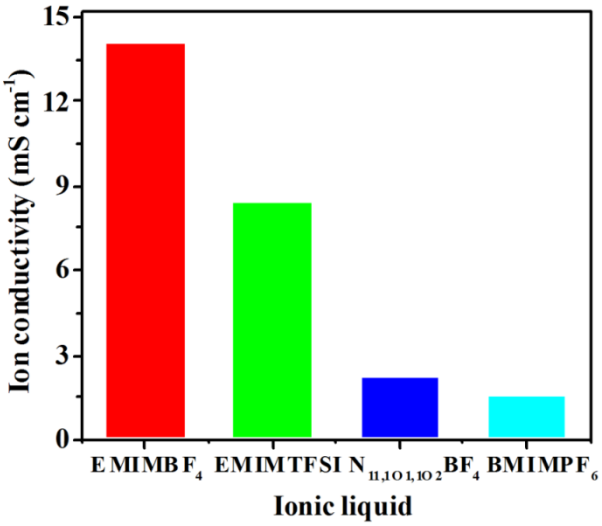

Fig. S13 Ionic conductivities of various ionic liquids including $EMIMBF_4$,[6] EMIMTFSI,[7] $N_{11,1O1,1O2}BF_4$,[8] and $BMIMPF_6$.[9]

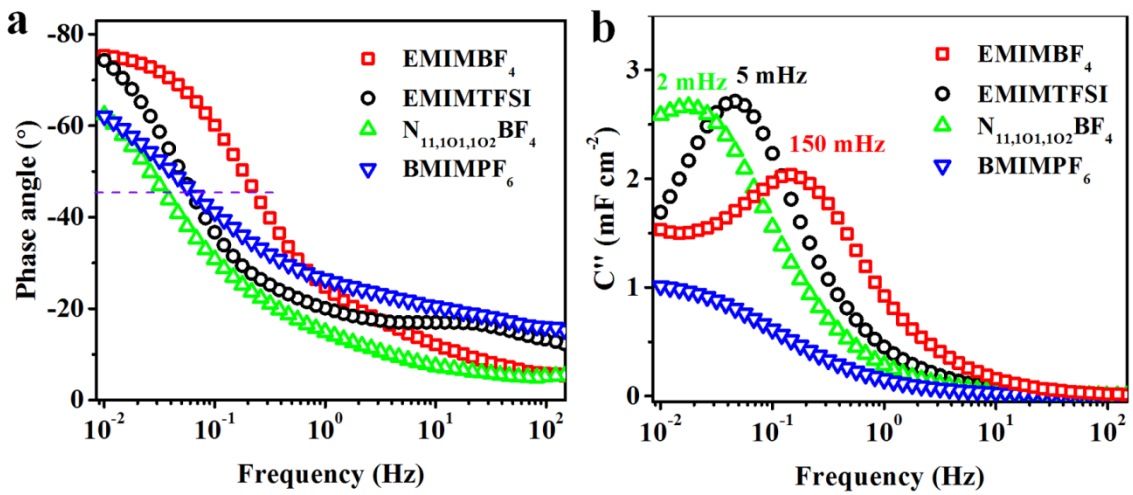

Fig. S14 (a) Bode plots and (b) imaginary capacitance of PM-MSCs-EB, PM-MSCs-ET, PM-MSCs-NB and PM-MSCs-BP, respectively.

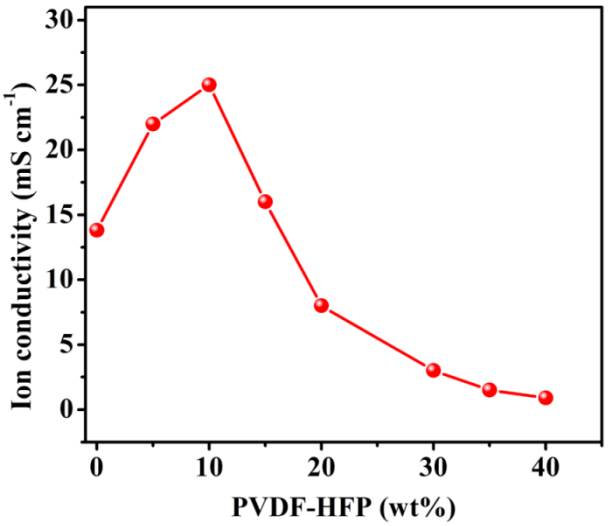

Fig. S15 Ionic conductivity of $EMIMBF_4$/PVDF-HFP ionogel electrolyte as a function of percentage content of PVDF-HFP.

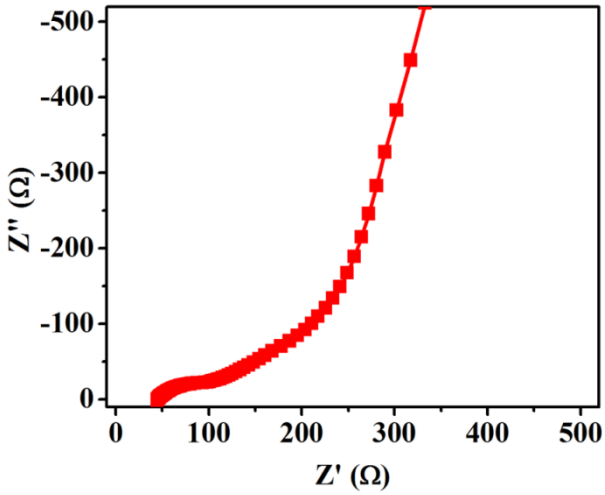

Fig. S16 EIS spectra of PM-MSCs-EBIE, showing a lower ESR of 45 Ω.

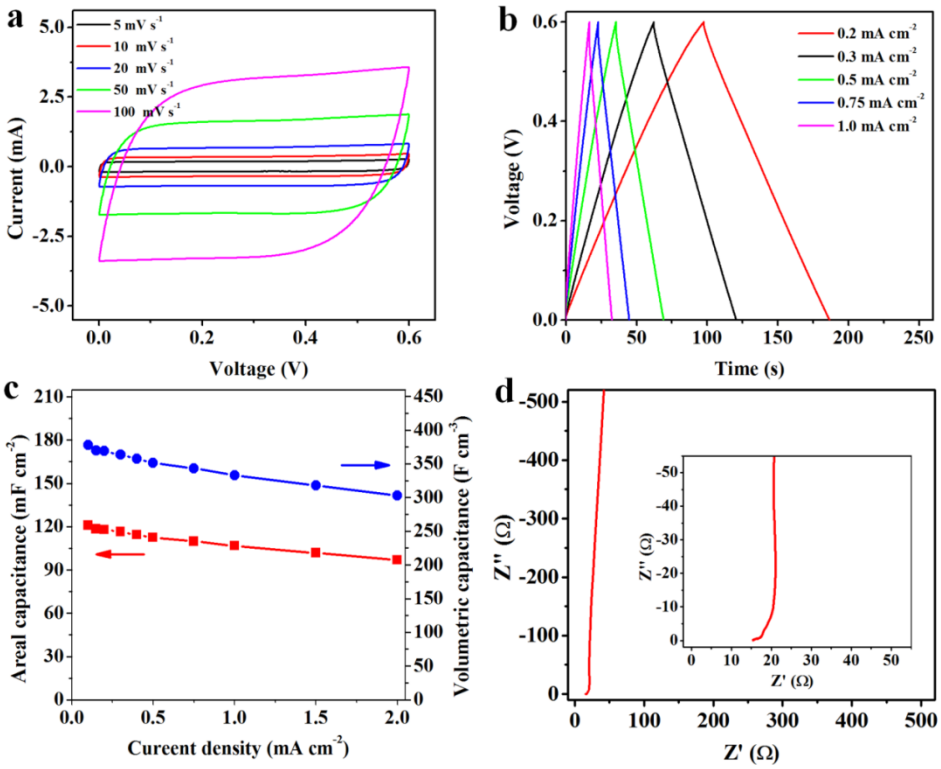

Fig. S17 Electrochemical performance of PM-MSCs tested at 1 M H_2SO_4 (denoted as PM-MSCs-SA). (a) CV curves, (b) GCD profiles, (c) Areal capacitance and volumetric capacitance, and (d) EIS spectra.

As shown in Fig. S14a and b, the rectangle-shaped CV curves and symmetric triangle-shaped GCD profiles exhibited representative capacitive behavior of PM-MSCs-SA at a cell voltage of 0.6 V. Remarkably, PM-MSCs-SA showed high areal capacitance of 121 mF $cm^{-2}$and volumetric capacitance of 378 F cm^{-3}, respectively, at current density of 0.1 mA cm^{-2} (Fig. S14c). Even at high current density of 2.0 mA cm^{-2}, areal capacitance of 97 mF cm^{-2} and volumetric capacitance of 303 F cm^{-3} were remained. Moreover, PM-MSCs-SA exhibited a low ESR of 15 Ω (Fig. S14d). However, PM-MSCs-SA delivered low areal and volumetric energy density of 1.5 μWh cm^{-2} and 4.7 mWh cm^{-3}, respectively, resulting from the narrow cell voltage of 0.6 V.

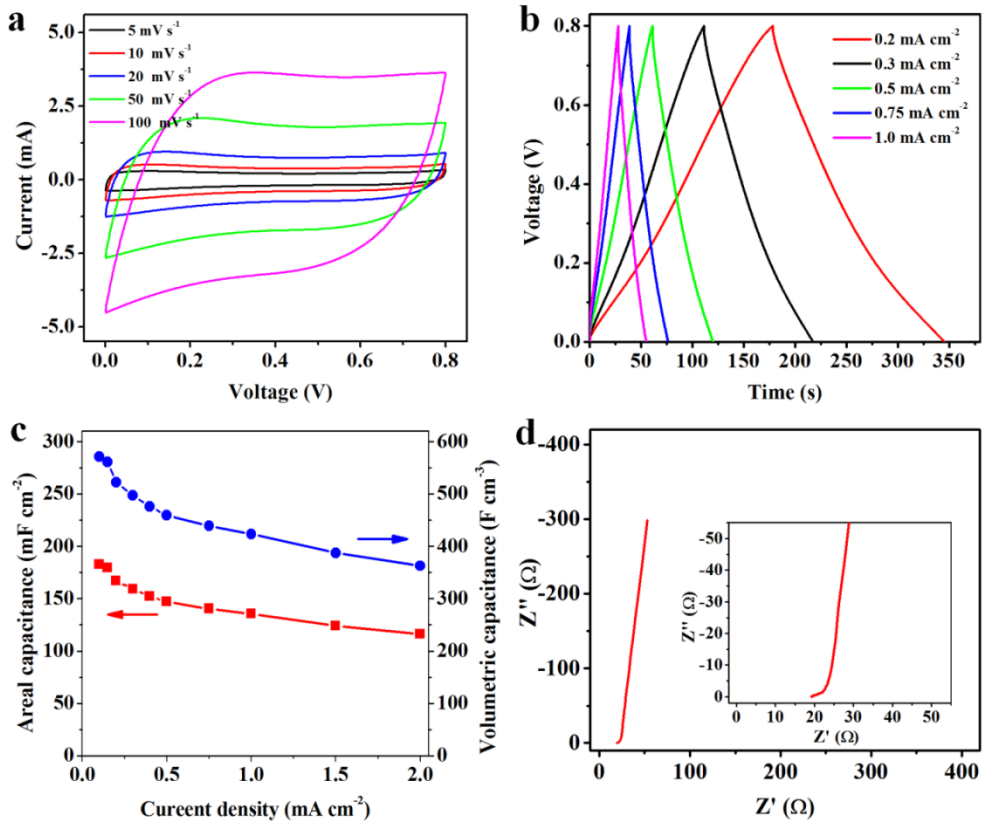

Fig. S18 Electrochemical performance of PM-MSCs measured at PVA/H_2SO_4 gel electrolyte (denoted as PM-MSCs-PSA). (a) CV curves, (b) GCD profiles, (c) areal capacitance and volumetric capacitance, and (d) EIS spectra.

From box-shaped CV curves (Fig. S15a) and symmetric GCD profiles (Fig. S15b), PM-MSCs-PSA with a voltage window of 0.8 V exhibited areal and volumetric capacitance of 183 mF cm^{-2} and 571 F cm^{-3} (Fig. S15c), respectively. Moreover, PM-MSCs-PSA showed low ESR of 19 Ω (Fig. S15d). Similar to PM-MSCs-SA, PM-MSCs-PSA also delivered low areal and volumetric energy density of 4.1 μWh cm^{-2} and 12.7 mWh cm^{-3}, respectively.

Table S1. Comparison of areal energy density of the state-of-the-art MXene based MSCs.

MSCs	Thickness (μm)	Electrolyte	Voltage (V)	C_{device}^{areal} (mF cm^{-2})	P_{device} (mW cm^{-2})	E_{device} (μWh cm^{-2})	Refs
MXene-EG	3.2	$EMIMBF_4$	3.0	11.2	4.5	14.0	This work
MXene-EG	3.2	$EMIMBF_4$/PVDF-HFP	3.0	10.7	3	13.4	This work
MXene-EG	3.2	EMIMTFSI	3.0	7.5	2.3	9.3	This work
MXene-EG	3.2	$N_{11,1O1,1O2}BF_4$	3.0	8.3	1.5	10.4	This work
HF-etched MXene	125	PVA/H_2SO_4	0.6	6.2	3.3	0.21	10
Clay-like MXene	125	PVA/H_2SO_4	0.6	25	46.6	0.76	10
MXene	/	PVA/KOH	0.6	25	0.74	1.25	11
MXene//Co-Al-LDH	/	6 M KOH	1.5	40	1.1	10.8	11
MXene//Co-Al-LDH	/	PVA/KOH	1.5	28.5	0.77	8.8	11
MXene	1.3	PVA/H_2SO_4	0.6	27.3	/	1.4	12
MXene (Ti_3CN)	0.7	PVA/H_2SO_4	0.6	8.4	0.1	0.4	3
MXene	0.7	PVA/H_2SO_4	0.6	14.2	0.4	0.8	3
MXene-rGO	/	PVA/H_2SO_4	0.6	34.6	0.18	2.2	13
MXene	/	PVA/H_3PO_4	0.6	22	/	1.1	14
MXene//rGO	0.3	PVA/H_2SO_4	1.0	2.4	/	1.6	15
MXene	1	PVA/H_3PO_4	0.8	3.3	/	0.3	16
MXene	2.2	PVA/H_2SO_4	0.6	29.3	/	1.5	17

Table S2. Comparison of volumetric energy density of the state-of-the-art MXene based MSCs.

MSCs	Electrolyte	Voltage (V)	$C_{device}^{volumetric}$ (F cm^{-3})	P_{device} (mW cm^{-3})	E_{device} (mWh cm^{-3})	Refs
MXene-EG	$EMIMBF_4$	3.0	35	14060	43.7	This work
MXene-EG	$EMIMBF_4$/PVDF-HFP	3.0	33.4	9300	41.8	This work
MXene-EG	EMIMTFSI	3.0	23.4	7000	29.1	This work
MXene-EG	$N_{11,1O1,1O2}BF_4$	3.0	26	4600	32.4	This work
MXene	PVA/H_2SO_4	0.6	357	15000	18	12
MXene	PVA/H_3PO_4	0.6	/	746	2.8	14
MXene//rGO	PVA/H_2SO_4	1.0	80	10000	8.6	15
MXene-EG	PVA/H_2SO_4	0.8	33	~800	3.5	16
MXene	PVA/H_2SO_4	0.6	119	1000	6.1	17
MXene	1M H_2SO_4	1	49.6	144	0.2	18

References

1 F. Shahzad, M. Alhabeb, C. B. Hatter, B. Anasori, S. Man Hong, C. M. Koo and Y. Gogotsi, *Science*, 2016, **353**, 1137-1140.

2 Y. Xia, T. S. Mathis, M.-Q. Zhao, B. Anasori, A. Dang, Z. Zhou, H. Cho, Y. Gogotsi and S. Yang, *Nature*, 2018, **557**, 409-412.

3 C. Zhang, M. P. Kremer, A. Seral-Ascaso, S.-H. Park, N. McEvoy, B. Anasori, Y. Gogotsi and V. Nicolosi, *Adv. Funct. Mater.*, 2018, **28**, 1705506.

4 Y. L. Zhong and T. M. Swager, *J. Am. Chem. Soc.*, 2012, **134**, 17896-17899.

5 F. Zhou, H. Huang, C. Xiao, S. Zheng, X. Shi, J. Qin, Q. Fu, X. Bao, X. Feng, K. Müllen and Z.-S. Wu, *J. Am. Chem. Soc.*, 2018, **140**, 8198-8205.

6 J. Fuller, R. T. Carlin and R. A. Osteryoung, *J. Electrochem. Soc.*, 1997, **144**, 3881-3886.

7 A. B. McEwen, H. L. Ngo, K. LeCompte and J. L. Goldman, *J. Electrochem. Soc.*, 1999, **146**, 1687-1695.

8 Z. Chen, S. Liu, Z. Li, Q. Zhang and Y. Deng, *New J. Chem.*, 2011, **35**, 1596-1606.

9 J. A. Widegren, E. M. Saurer, K. N. Marsh and J. W. Magee, *J. Chem. Thermodyn.*, 2005, **37**, 569-575.

10 N. Kurra, B. Ahmed, Y. Gogotsi and H. N. Alshareef, *Adv. Energy Mater.*, 2016, **6**, 1601372.

11 S. Xu, Y. Dall'Agnese, G. Wei, C. Zhang, Y. Gogotsi and W. Han, *Nano Energy*, 2018, **50**, 479-488.

12 Y.-Y. Peng, B. Akuzum, N. Kurra, M.-Q. Zhao, M. Alhabeb, B. Anasori, E. C. Kumbur, H. N. Alshareef, M.-D. Ger and Y. Gogotsi, *Energy Environ. Sci.*, 2016, **9**, 2847-2854.

13 Y. Yue, N. Liu, Y. Ma, S. Wang, W. Liu, C. Luo, H. Zhang, F. Cheng, J. Rao, X. Hu, J. Su and Y. Gao, *ACS Nano*, 2018, **12**, 4224-4232.

14 Q. Jiang, C. S. Wu, Z. J. Wang, A. C. Wang, J. H. He, Z. L. Wang and H. N. Alshareef, *Nano Energy*, 2018, **45**, 266-272.

15 C. Couly, M. Alhabeb, K. L. V. Aken, N. Kurra, L. Gomes, A. M. Navarro‐Suárez, B. Anasori, H. N. Alshareef and Y. Gogotsi, *Adv. Electron. Mater.*, 2018, **4**, 1700339.

16 H. Li, Y. Hou, F. Wang, M. R. Lohe, X. Zhuang, L. Niu and X. Feng, *Adv. Energy Mater.*, 2017, **7**, 1601847.

17 H. B. Hu and T. Hua, *J. Mater. Chem. A*, 2017, **5**, 19639-19648.

18 B.-S. Shen, H. Wang, L.-J. Wu, R.-S. Guo, Q. Huang and X.-B. Yan, *Chinese Chem. Lett.*, 2016, **25**, 1586-1591.